J Mater Sci: Mater Electron (2007) 18:1131–1136
DOI 10.1007/s10854-007-9144-5

Multiwalled carbon nanotubes embedded in sol–gel derived TiO_2 matrices and their use as room temperature gas sensors

M. Sánchez · R. Guirado · M. E. Rincón

Received: 16 January 2007 / Accepted: 6 February 2007 / Published online: 28 February 2007

Abstract Sol–gel TiO_2/Multiwall Carbon Nanotubes composites obtained by the Ti-isopropoxide route are reported as room temperature sensitive coatings. The effect of functionalizing the carbon nanotubes in strong oxidizing acids prior to the sol–gel synthesis is studied in the detection of acetone (CH_3COCH_3) and ammonia (NH_3). Although, mixed oxide phases were found in the sol–gel oxide and composites, sensing was highly reproducible in the composites, with fast adsorption/desorption cycles at room temperature. Composites based on as-received multiwalled carbon nanotubes show an increase in films resistance during acetone and ammonia adsorption, while composites based on functionalized carbon nanotubes show longer acetone desorption times and a decrease in resistance during ammonia sensing. Acetone sensing in both composites contrast with the slight decrement in resistance observed in either pure titanium oxide or carbon nanotubes, in agreement with preliminary theoretical results. In contrast, the strong dependence of NH_3 to the presence of oxygen and hydroxyl atoms on the carbon nanotube surface is not well understood.

1 Introduction

Room temperature desorption has been one of the limitations of molecular sensors based on multiwalled carbon nanotubes (MWCNTs) [1–4], therefore pursuing the design of hybrid materials with potential applications as efficient molecular sensors has become an active area of research. In particular, the activity of TiO_2 loaded CNT's towards small gaseous molecules has not been tested, even though both compounds as separated systems have been extensively studied as possible gas sensors [5–9].

We believe that combining MWCNT with electrochemically active sol–gel oxides renders a more complex system that needs to be experimentally and theoretically addressed. In this work we will particularly discuss the role played by the presence of mixed oxide phases, typical of some sol–gel synthesis, and the different degree of functionalization/purification of the carbon nanotubes in the sensing properties of the samples. In a previous contribution [10] we could not clearly asses the relevance of functionalization, due to the different sol–gel routes used for the composites. Nevertheless, our theoretical calculations indicated that the magnitude and direction of charge transfer between acetone molecules and the carbon nanotube surface might considerably vary depending on the degree of oxygen coordinated around Ti sites, leading to contrasting resistance variations.

M. Sánchez · M. E. Rincón (✉)
Centro de Investigación en Energía, Universidad Nacional Autónoma de México, Apartado Postal 34, Temixco, MOR 62580, Mexico
e-mail: merg@cie.unam.mx

R. Guirado
Instituto de Física "Manuel Sandoval Vallarta"–UASLP, Álvaro Obregón 64, San Luis Potosí, SLP 78000, Mexico

2 Experimental

2.1 MWCNT functionalization

Commercially available MWCNT's (Nanostructured & Amorphous Materials Inc., outer diameter 3–10 nm, non-alligned, 80% purity), were subjected to conventional acid treatment, placing 0.1 g MWCNTs in a

mixture composed of 2.5 M HNO_3 and 0.5 M H_2SO_4, and refluxing at 100 °C for 6 h. The resulting suspension was filtered and the solids dispersed in 3 M HCl, refluxed again at 100 °C for 5 h. After the combined acid treatment the yield of functionalized MWCNT was 90–95%.

2.2 Sol–gel synthesis of TiO_2–MWCNT composites

Titanium oxide and TiO_2–MWCNT composites were prepared by sol–gel techniques, using titanium tetraisopropoxide [$Ti(C_3H_6OH)_4$, Sigma-Aldrich 97%], as the precursor, and 2-propanol (Sigma-Aldrich 99%) as the solvent. To obtain 1 g TiO_2, 4 mL Ti-Isopropoxide were added drop by drop to a mixture containing 4 mL HCl (Merck 37.1 wt.%) and 46 mL 2-propanol. The solution was kept under strong stirring at room temperature for 24 h, and then the solvent was evaporated at 70 °C for 24 h. The solids were dried at 400 °C in air for 1 h, and used in a serigraphic paste containing few drops of Triton-X and propylene glycol. Corning glass substrates (1″×3″) were thoroughly washed and used as substrates for screen-printed coatings. The films were annealed at 400 °C in air for 1 h to eliminate the organic compounds (i.e., Triton-X and propylene glycol) and to induce crystallinity on the sol–gel oxides. For composites, the procedure is basically the one described for the oxides, except that the mixture of HCl and alcohol contained the required amount of MWCNTs and the dispersion and adequate mixing of the components was enhanced by stirring the solution in an ultrasonic bath for 30–40 min previous to the addition of the titanium precursor. The crystalline structure of the sol–gel TiO_2/MWCNT composites was investigated by X-ray diffraction (XRD) analysis performed using a Rigaku Dmax 2200 equipment with Cu–Kα (λ = 0.15405 nm) radiation. Film thickness was in the range of 3–4 μm and % CNTs in the range of 0–10 wt.% to minimize carbon agglomeration. From this concentration range, the composites containing 0.1 g of MWCNTs (10 wt.%) were above the percolation threshold and selected due to faster adsorption/desorption times.

2.3 Gas measurements

The equipment used for sensing is depicted in Fig. 1. To get a baseline at room temperature, air was pumped at 7 L/min for several minutes. During measurements, acetone vapour was obtained from a bubbler operated with 150 mL/min nitrogen flow rate. Experiments were conducted under saturated vapour conditions, using different ratios of acetone/water solution to change the concentration of acetone in the gas flow. Water interference was verified and discarded as a possible source of error in the concentration range tested. A measuring cycle consisted of the time required to monitor the changes in resistance due to acetone adsorption and the time required to pump out the vapour from the glass chamber, flushing it with air. There was a few minutes break between cycles, and for a typical run, 5 cycles were run with good reproducibility. Electrical contacts were made with silver paint using parallel lines with 5 mm length and 5 mm separation to obtain a square configuration. A Keithley 2000 digital multimeter was employed to continuously monitor changes in the resistance values during exposure to acetone. The square configuration let us use the sheet resistance ($R_\square$) as a variable independent of the area monitored.

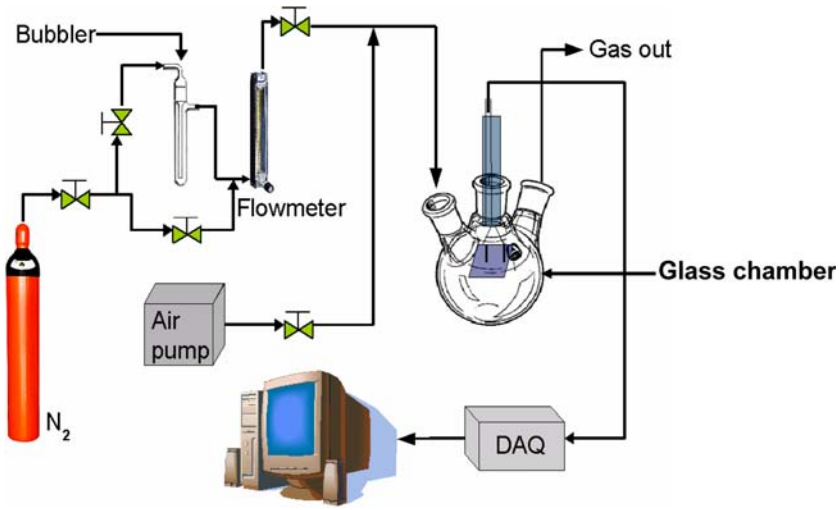

Fig. 1 Schematic diagram of the system used to test sensor response. Nitrogen gas is saturated with acetone at the bubbler and injected into the test chamber. There, changes in sensor resistance are monitored during acetone adsorption and when cutting the acetone-N_2 flow and flushing the test chamber with air

2.4 Theoretical calculations

We performed ab initio Hartree-Fock (HF) and density functional theory (DFT) calculations analyzing the acetone adsorption on a model (5,5) carbon nanotube containing small Ti_xO_y (x = 1 – 3, y = 2,4,6) clusters adsorbed on its surface. We fully optimized our considered systems using the HF method (using the minimal STO-3G basis set) and then, in a second step, we used these optimized molecular geometries to perform DFT calculations (considering the B3LYP expression for the exchange-correlation potential) to obtain the charge distribution on each site of the structure.

3 Results and discussion

3.1 Structural characterization

The XRD patterns of TiO_2 and TiO_2/MWCNTs are shown in Fig. 2. Figure 2(a) shows the crystalline structure of the oxide, Fig. 2(b) the pattern of composites based in 10 wt.% as-received MWCNT, Fig. 2(c) the pattern of composites based on 10 wt.% functionalized MWCNTs. Although the presence of anatase, brookite, and rutile, (labelled A, B, and R, I in the figure) is observed in all the samples, it is notorious the large intensity of rutile peaks in composites based on as-received MWCNTs. On the other hand, functionalized MWCNTs favour the formation of anatase and brookite over rutile. This is better illustrated in Fig. 3, where the crystallographic composition of the samples is compared. These percentages were calculated according to the following equations [11]:

$$W_A = k_A A_A/(k_A A_A + A_R + k_B A_B) \quad (1a)$$

$$W_R = A_R/(k_A A_A + A_R + k_B A_B) \quad (1b)$$

$$W_B = k_B A_B/(k_A A_A + A_R + k_B A_B) \quad (1c)$$

Here, $k_A = 0.88$, $k_B = 2.72$, A_A, A_R, and A_B, are the intensities of the main diffraction peaks of anatase ($2\theta = 25.2°$), rutile ($2\theta = 27.3°$), and brookite ($2\theta = 30.8°$), respectively.

3.2 Room temperature sensing

The response of mixed-oxide TiO_2 and MWCNT coatings to nitrogen flow containing 1 vol.% acetone was tested at room temperature and presented in Fig. 4(a) and 4(b), respectively. In the figure the concentration of acetone is represented by the dashed line and the changes in resistance ($\Delta R = R_{vapour} - R_{baseline}$) plotted as a function of adsorption and desorption times. The small decrease in films resistance during acetone adsorption indicates *n*-type doping for the oxide film (electron transfer from acetone to TiO_2), an *p*-type doping for oxidized MWCNTs (electron transfer from MWCNTs to acetone). Similarly, Fig. 4 (c–d) compares the response of sol–gel composites based on as-received and functionalized MWCNTs. It is notorious the increase in resistance of both composites when sensing acetone which contrast with the reduce resistance observed in their components. Moreover, the signal saturates on the acetone cycle in the composite based on functionalized MWCNT (saturation limit below 1%) but not on the composite based on as-received MWCNTs (saturation limit above 1%). This difference could be related to the different oxide

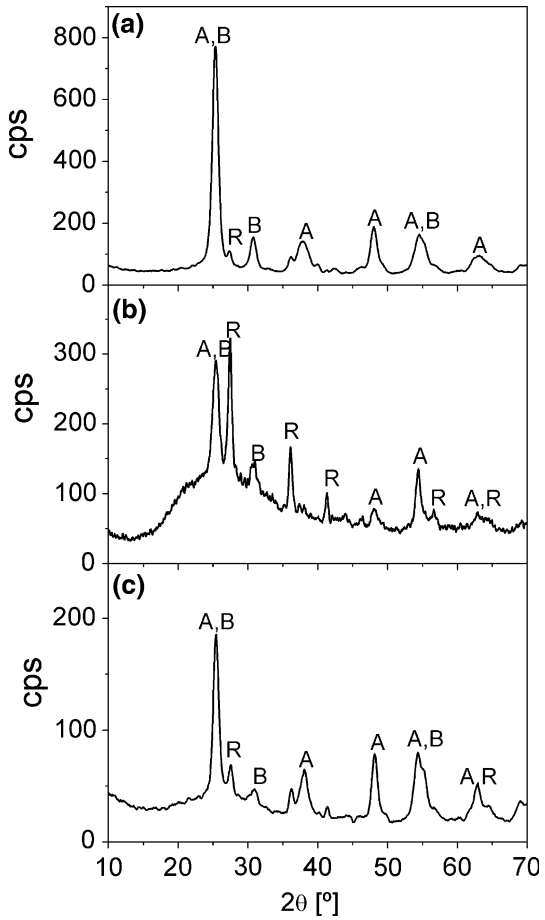

Fig. 2 XRD patterns of screen printed films annealed in air at 400 °C for 1 h. (**a**) TiO_2-isopropoxide route, (**b**) TiO_2/as-received MWCNTs, (**c**) TiO_2/functionalized MWCNTs. The composites contained 10 wt.% multiwalled carbon nanotubes. For functionalization, the as-received MWCNTs were refluxed in 2.5 M HNO_3/0.5 M H_2SO_4 for 6 h, followed by treatment in HCl 3 M for 5 h. A = anatase, B = brookite, R = rutile

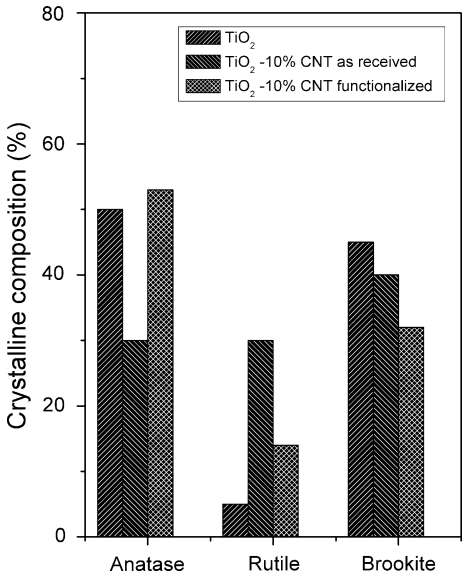

Fig. 3 Crystalline composition of the various samples air annealed at 400 °C for 1 h

matrix surrounding the MWCNTs (see Fig. 2), since there are clear structural differences between the composites. Anatase and brookite were also the dominant crystalline phases on the oxide sample (Fig. 2a) and per se do not seem to have an important role during acetone sensing. The purification/functionalization of MWCNTs incorporates oxygenated functional groups on the carbon surface due to the treatment with HNO_3/H_2SO_4. We believe that the structural differences indicate a different type of interaction (bonding) between the carbon nanotube and the oxide in the as-received and functionalized MWCNTs. The presence of oxygen in the carbon surface apparently causes a uniform oxide growth, which manifest as a superior films resistance and also as slower desorption rate of acetone (see Table 1). Nevertheless, both composites show room temperature acetone desorption in the minutes scale, which contrast with the slow desorption of sensors based on MWCNTs [9, 12].

To further support the differences observed in both composites, detection of NH_3 is presented in Fig. 5. Here again, the saturation limit of the composite based on functionalized MWCNTs (<2 vol.% NH_3) is much lower than the one based in as received MWCNTs (>60 vol.% NH_3). Moreover, with this reducing gas, both composites show contrasting resistance variations. The increase in resistivity agrees with the *p*-type response reported for functionalized MWCNTs containing metals like Co, Fe and Al [4], which in our case are present in the as-received MWCNTs; without metals, functionalized MWCNTs have weak and slow responses but the authors did not report if an inversion in the signal is also observed. In contrast, the TiO_2/10 wt.% functionalized MWCNTs composite have strong and fast responses at low NH_3 concentration.

Previous theoretical results indicate that the presence of structural defects and chemical impurities, as

Table 1 Adsorption and desorption times for acetone

Sample	$t_{adsorption}$ (s)	$t_{desorption}$ (s)
TiO_2	90	90
MWCNT	120	120
TiO_2/10 wt.% MWCNT as received	30–40	10–20
TiO_2/10 wt.% MWCNT functionalized	~10	300

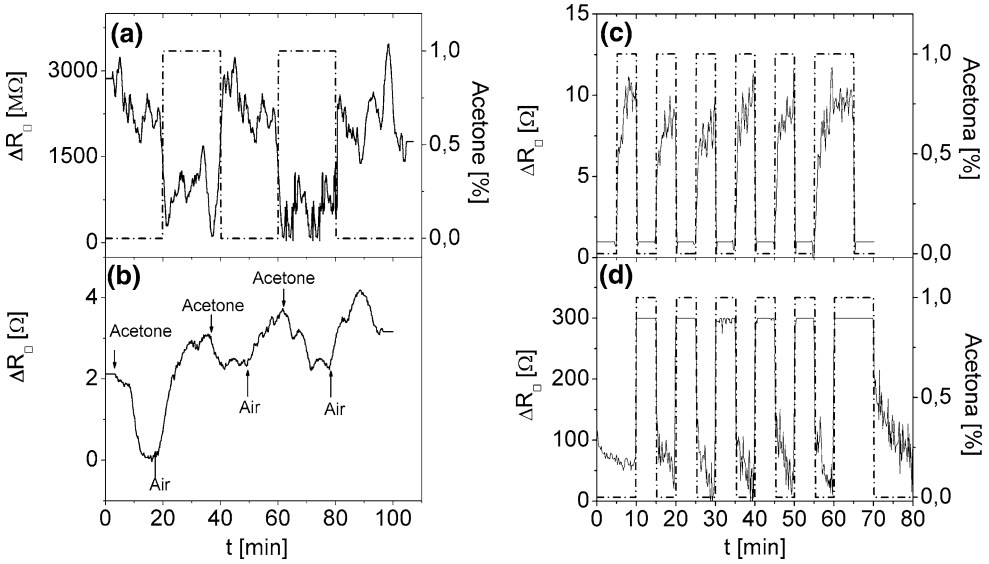

Fig. 4 Changes in resistance versus acetone adsorption/desorption times: (**a**) TiO_2; (**b**) oxidized MWCNTs; (**c**) TiO_2/10 wt.% as received MWCNTs; (**d**) TiO_2/10 wt.% functionalized MWCNTs. Coatings exposed to 150 mL/min N_2 flow with 1 vol.% acetone concentration as indicated by the dashed line

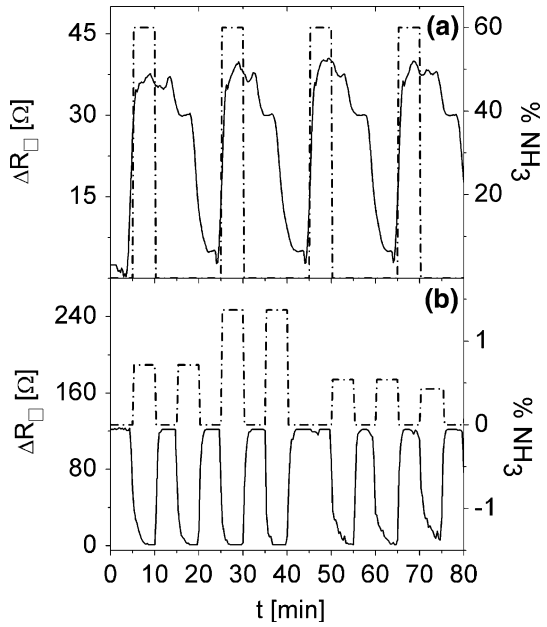

Fig. 5 Changes in resistance versus NH_3 adsorption/desorption times: (**a**) TiO_2/10 wt.% as received MWCNTs; (**b**) TiO_2/10 wt.% functionalized MWCNTs. Coatings exposed to 150 mL/min N_2 flow with vol.% NH_3 concentration as indicated by the dashed line

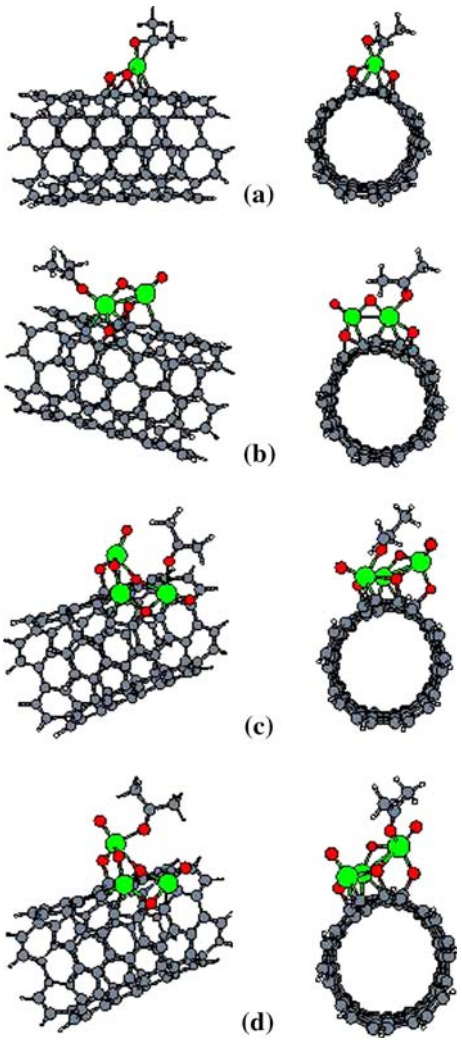

Fig. 6 Ab initio low energy atomic configurations for acetone adsorption on Ti_xO_y-doped carbon nanotubes. In the right column we show the corresponding side view of the equilibrium arrays. (**a**) TiO_2, (**b**) Ti_2O_4, and (**c**–**d**) Ti_3O_6 clusters. O (red), Ti (green), C (gray), H (white)

well as the existence of surface regions with different curvature, may favour the attachment of well defined molecular species [13–16]. Therefore, in previous work [10] aiming to understand the effect of different sol–gel baths, we performed theoretical calculations considering both bare and chemically functionalized carbon nanotubes, the latter being characterized by the presence of adsorbed oxygen and titanium atoms, hydroxyl species, together with some small TiO_2, Ti_2O_4, and Ti_3O_6 clusters. Figure 6 reproduces some of the ab initio lowest energy atomic configurations obtained when a single CH_3COCH_3 molecule interacts with small TiO_2 [Fig 6(a)], Ti_2O_4 [Fig 6(b)], and Ti_3O_6 [Figs. 6(c) and 6(d)] clusters deposited on our model (5, 5) carbon nanotube. The structure illustrated in Fig 6(a), a chemisorbed configuration in which the Ti add-atom is bonded to both O and C species of the CH_3COCH_3 group, results in the formation of a negatively charged acetone (–0.33*e*) and does not follows the here-reported resistance variations in which electron injection to the nanotube is required in order to explain our measured data. Interestingly, as the size of the deposited Ti_xO_y clusters increases (Figs. 6(b), 6(c), and 6(d)), only single bonded configurations are obtained and in these the direction for the charge transfer supports our experimental data (acetone → Ti_xO_y/carbon nanotube). Moreover, the presence of Ti atoms attached to the carbon nanotube through an oxygen atom occurs as the size of the cluster increases and it is more representative of the synthesis based on functionalized MWCNTs. Preliminary data for NH_3 adsorption (not shown) predicts an increase in resistivity for the structures presented in Fig 6. We proposed that detection of NH_3 might be also possible through the inter-tube modulation effect (i.e., MWCNT–TiO_2/NH3–MWCNT junctions), which is shown in Fig. 7 and where titania is acting as a buffer layer to avoid MWCNTs de-doping (the energy scale in this diagram comes from well accepted values for TiO_2 and functionalized MWCNTs [17]). The question of why this only occurs in composites based in functionalized MWCNTs is under study.

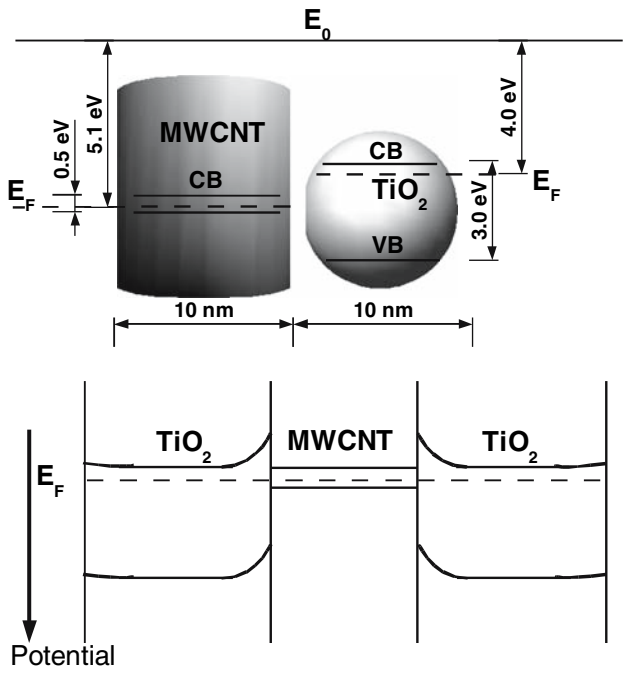

Fig. 7 Estimate of the junction properties of TiO_2–MWCNT–TiO_2 which can be affected by the adsorption of gases

4 Conclusion

The detection of acetone and NH_3 was found to be possible at ambient temperature with TiO_2/MWNT gas sensors fabricated by the sol–gel method. Acid treatment was found to improve the sensing potential of MWCNTs, particularly the magnitude of the change in resistance, forecasting lower detection limits for both gases. Acetone desorption rates seem superior in composites based in as-received MWCNT, but not in NH_3 desorption. Theoretical ab initio calculations predicted an inversion in the acetone $\rightarrow$ Ti_xO_y/carbon nanotube charge transfer direction as the size of the oxide cluster increases, explaining the inverse changes in resistance of the composites versus the components, but have not been successful in explaining the differences observed in the composites during NH_3 adsorption.

Acknowledgments Financial support from DGAPA-UNAM (IN111106-3) is gratefully acknowledged, as well as the fellowship (M. Sánchez) provided by CONACYT-México. We thank R. Morán and M.L. Román for technical assistance and XRD analyses. R.A.G.-L. would like to acknowledge the financial support from CONACyT-Mexico under project 45928-F.

References

1. K..G. Ong, K. Zeng, C.A. Grimes, IEEE Sensors J. **2**, 82 (2002)
2. F. Villalpando-Páez, A.H. Romero, E. Muñoz-Sandoval, L.M. Martínez, H. Terrones, M. Terrones, Chem. Phys. Lett. **386**, 137 (2004)
3. L. Valentini, C. Cantalini, I. Armentano, J.M. Kenny, L. Lozzi, S. Santucci, Diamond Relat. Mater. **13**, 1301 (2004)
4. R. Ionescu, E.H. Espinosa, E. Sotter, E. Llobet, X. Vilanova, X. Correig, A. Felten, C. Bittencourt, G. Van Lier, J.C. Charlier, J.J. Pireaux, Sens. Actuators B **113**, 36 (2006)
5. P.J.D. Lindan, N.M. Morrison, Phys. Rev. Lett. **80**, 762 (1998)
6. L.L.W. Chow, M.M.F. Yuen, P.C.H. Chan, A.T. Cheung, Sens. Actuators. B **76**, 310 (2001)
7. N.O. Savage, S.A. Akbar, P.K. Dutta, Sens. Actuators B **72**, 239 (2001)
8. M. Ferroni, M.C. Carotta, V. Guidi, G. Martinelli, F. Ronconi, M. Sacerdoti, E. Traversa, Sens. Actuators B **77**, 163 (2001)
9. A. Ruiz, A. Cornet, J.R. Morante, Sens. Actuators B **100**, 256 (2004)
10. R.A. Guirado-López, M. Sánchez, M.E. Rincón, J. Phys. Chem. C, in press
11. H. Zhang, J.F. Banfield, J. Phys. Chem. B **104**, 3481 (2000)
12. A.M. Taurino, S. Capone, A. Boschetti, T. Toccoli, R. Verucchi, A. Pallaoro, P. Siciliano, S. Iannota, Sens. Actuators B. **100**, 177 (2004)
13. J. Li, Y. Lu, Q. Ye, M. Cinke, J. Han, M. Meyyappan, Nano Lett. **3**, 929 (2003)
14. M.K. Kostov, E.E. Santiso, A.M. George, K.E. Gubbins, M. Buongiorno-Nardelli, Phys. Rev. Lett. **95**, 136105 (2005)
15. S. Dag, Y. Ozturk, S. Ciraci, T. Yildirim, Phys. Rev. B **72**, 155404 (2005)
16. B. Gómez, J.M. Martínez-Magadan, J. Phys. Chem. B **109**, 14868 (2005)
17. H. Ago, T. Kugler, F. Cacialli, W.R. Salaneck, M.S.P. Shaffer, A.H. Windle, R.H. Friend, J. Phys. Chem. B **103**, 8116 (1999)